Published in final edited form as:
Biochemistry. 2002 March 26; 41(12): 3991–4001.

Molecular Features of the Copper Binding Sites in the Octarepeat Domain of the Prion Protein†

Colin S. Burns§, **Eliah Aronoff-Spencer**§, **Christine M. Dunham**§, **Paula Lario**, **Nikolai I. Avdievich**, **William E. Antholine**, **Marilyn M. Olmstead**, **Alice Vrielink**, **Gary J. Gerfen**, **Jack Peisach**, **William G. Scott**, and **Glenn L. Millhauser***
Department of Chemistry and Biochemistry, University of California, Santa Cruz, California 95064, Department of Physiology and Biophysics, Albert Einstein College of Medicine, 1300 Morris Park Avenue, Bronx, New York 10461, Biophysics Research Institute, Medical College of Wisconsin, Milwaukee, Wisconsin 53226, and Department of Chemistry, University of California, Davis, California 95616

Abstract

Recent evidence suggests that the prion protein (PrP) is a copper binding protein. The N-terminal region of human PrP contains four sequential copies of the highly conserved octarepeat sequence PHGGGWGQ spanning residues 60–91. This region selectively binds Cu^{2+} in vivo. In a previous study using peptide design, EPR, and CD spectroscopy, we showed that the HGGGW segment within each octarepeat comprises the fundamental Cu^{2+} binding unit [Aronoff-Spencer et al. (2000) *Biochemistry 40*, 13760–13771]. Here we present the first atomic resolution view of the copper binding site within an octarepeat. The crystal structure of HGGGW in a complex with Cu^{2+} reveals equatorial coordination by the histidine imidazole, two deprotonated glycine amides, and a glycine carbonyl, along with an axial water bridging to the Trp indole. Companion S-band EPR, X-band ESEEM, and HYSCORE experiments performed on a library of ^{15}N-labeled peptides indicate that the structure of the copper binding site in HGGGW and PHGGGWGQ in solution is consistent with that of the crystal structure. Moreover, EPR performed on PrP(23–28, 57–91) and an ^{15}N-labeled analogue demonstrates that the identified structure is maintained in the full PrP octarepeat domain. It has been shown that copper stimulates PrP endocytosis. The identified Gly–Cu linkage is unstable below pH ≈6.5 and thus suggests a pH-dependent molecular mechanism by which PrP detects Cu^{2+} in the extracellular matrix or releases PrP-bound Cu^{2+} within the endosome. The structure also reveals an unusual complementary interaction between copper-structured HGGGW units that may facilitate molecular recognition between prion proteins, thereby suggesting a mechanism for transmembrane signaling and perhaps conversion to the pathogenic form.

A misfolded form of the prion protein (PrP)[1] is responsible for the transmissible spongiform encephalopathies (TSEs), including mad cow disease (BSE) and Creutzfeldt–Jakob disease (CJD) in humans (1). Despite nearly 20 years of PrP research, the physiological function of

†This work was supported by NIH Grants GM65790 (G.L.M.), GM60609 (G.J.G.), and GM40168 (J.P.) and by NSF Grant MCB-0090994 (W.G.S.).

*Correspondence should be addressed to this author. Telephone: (831) 459-2176. Fax: (831) 459-2935. glennm@hydrogen.ucsc.edu.
§These authors made equal contributions to this work.

[1]Abbreviations: PrP, prion protein; PrP^C, cellular isoform of PrP; PrP^{Sc}, scrapie isoform of PrP; PrP(57–91), residues 57 through 91 of PrP; EPR, electron paramagnetic resonance; ESEEM, electron spin–echo envelope modulation; HYSCORE, hyperfine sublevel correlation spectroscopy; e^2qQ/h, maximum quadrupole coupling; η, quadrupole asymmetry parameter; NQI, nuclear quadrupole interaction; DQ, double quantum; A_{iso}, isotropic component of the hyperfine coupling constant; T, anisotropic component of the hyperfine coupling constant; CD, circular dichroism; NMR, nuclear magnetic resonance; XAFS, X-ray absorption fine structure; GPI, glycosylphosphatidylinositol; NEM, *N*-ethylmorpholine; K_d, dissociation constant.

this remarkable protein is only now becoming clear. Recent work suggests that the membrane-bound prion protein binds copper in its N-terminal domain (2–11). It has been proposed that PrP participates in the regulation of copper (2,12,13) and possibly modulates the concentrations of reactive oxygen species (14–16). A hallmark of the PrP N-terminal domain is the octarepeat region, residues 60–91 in human and Syrian hamster PrP, which is composed of four or more repeats of the fundamental eight residue sequence PHGGGWGQ (Figure 1). Most current work suggests that copper binding takes place within this region and also in an adjacent region between the octarepeats and PrP's globular C-terminal domain. The octarepeat domain and copper have been implicated in neurological disease. Humans with PrPs containing extra octarepeats are predisposed to CJD (17). Elimination of the octarepeat domain slows disease progression (18). Addition of copper to wild-type PrP confers protease resistance, a property also characteristic of the pathogenic form (19).

There are ongoing efforts to determine how the octarepeat domain binds copper. The cellular, GPI-anchored, prion protein (PrP^{C}, Figure 1) exists predominantly on the extracellular membrane surface (20) where exchangeable copper is in the divalent oxidation state (21,22). Mass spectrometry studies performed at an extracellular pH of approximately 7.4 have demonstrated that peptides corresponding to the full octarepeat domain bind four Cu^{2+} ions with micromolar affinity (2,7), with significant cooperativity (2) and select for this species over other divalent metal ions (2). These findings have been confirmed in full-length PrP (23). Raman studies have suggested that each PHGGGWGQ octarepeat binds a single Cu^{2+} by a nitrogen from the His imidazole side chain and deprotonated amide nitrogens from the second and third glycines following the His (8). Alternatively, circular dichroism (CD) and electron paramagnetic resonance (EPR) studies on the peptides PHGGGWGQ and HGGG led to the conclusion that coordination within an octarepeat arises from the His imidazole and three amide nitrogens all within the HGGG unit (5).

In a study combining peptide design, CD, multifrequency EPR, and electron spin–echo envelope modulation (ESEEM) spectroscopy, we recently demonstrated that the peptide HGGGW bound to Cu^{2+} gave spectroscopic signatures that were indistinguishable from those of Cu^{2+}-bound multioctarepeat sequences (4). EPR and CD titration experiments demonstrated a rigorous 1:1 Cu^{2+}/octarepeat binding stoichiometry regardless of the number of octarepeats within a sequence. These findings led us to conclude that HGGGW comprises the fundamental Cu^{2+} binding unit. By comparing the EPR of HGGGW with that of HGG, we further concluded that nitrogen coordination was from the His imidazole and deprotonated amides from the next two glycines. Although the Trp in HGGGW was found to be essential in providing the proper coordination environment, it was not clear how this residue interacted with the Cu^{2+}.

Determining the precise Cu^{2+} coordination environment within the octarepeat domain is essential for advancing the understanding of PrP's role as a copper binding protein. Here we report the X-ray crystal structure of HGGGW in complex with Cu^{2+}. In addition, we determine whether the coordination environment identified in the crystal structure holds in solution for HGGGW, PHGGGWGQ, and the PrP octarepeat domain PrP(23–28, 57–91) using ESEEM, HYSCORE, and low-frequency S-band EPR. A library of ^{15}N-labeled PrP peptides was used in these EPR experiments to assign specific Cu–N couplings. These combined crystallographic and EPR studies provide the first atomic resolution view of the copper binding site within an octarepeat. In addition, the structural features allow us to hypothesize how PrP functions as a copper sensor or transporter, how octarepeats participate in transmembrane signaling, and how copper-mediated PrP recognition contributes to the formation of PrP^{Sc}.

Materials and Methods

Sample Preparation

HGGGW, the octarepeat (PHGGGWGQ), and PrP(23–28, 57–91) were prepared with an acetyl group at the N-terminus and amidated at the C-terminus. Methods for synthesis, purification, and characterization have been described previously (4). N-Fmocglycine(^{15}N, 98+%) was obtained from Cambridge Isotope Laboratories, Inc.

X-ray Crystallography

HGGGW in complex with Cu^{2+} was crystallized by the hanging-drop vapor diffusion method by the addition of a 2 μL sample solution (15 mg/mL, pH 7.4) to 2 μL of a reservoir solution containing 100 mM HEPES at pH 7.4 and 10–30% Jeffamine M-600. Crystals having dimensions 0.1 mm by 0.2 mm by 0.03 mm grew within 24 h. For cryoprotection, crystals were soaked in paratone and flash-cooled in a stream of liquid nitrogen. Crystals were mounted in the 92 K nitrogen cold stream provided by a CRYO Industries low-temperature apparatus on the goniometer head of a Bruker SMART 1000 diffractometer. Diffraction data were collected with graphite-monochromated Mo Kα radiation employing a 0.3° ω scan and approximately a full sphere of data to a resolution of 0.68 Å. An empirical correction for absorption was applied. A total of 10 657 reflections were collected, of which 8394 were unique [R(int) = 0.045] and 7581 were observed [$I > 2\sigma(I)$]. The structure was solved by direct methods and refined by full-matrix least-squares on F^2. All non-hydrogen atoms were refined with anisotropic thermal parameters. Hydrogen atoms were located on a difference map. The maximum and minimum peaks in the final difference Fourier map corresponded to 0.64 and −0.53 eÅ^{-3}, respectively. Crystal Data: $C_{25}H_{41}CuN_9O_{12}$, MM = 723.21, triclinic, *P1*, a = 8.7641(6) Å, b = 9.4145(7) Å, c = 10.8450(8) Å, α = 82.840(7)°, β = 79.744(7)°, γ = 62.342 (7)°, Z = 1. The refinement converged with a wR2 value of 0.082 using all data and an R1 value of 0.037 for the observed data using 431 parameters. Programs used were the SHELXTL 5.10 crystallographic software suite (Sheldrick, G. M.; Bruker Analytical X-ray Instruments, Inc.).

Electron Paramagnetic Resonance

All samples were prepared with degassed buffer containing 25 mM *N*-ethylmorpholine (NEM), 150 mM potassium chloride (KCl), and 20% glycerol (v/v) where the glycerol served as a cryoprotectant. ^{63}Cu (99.62%, Cambridge Isotope Laboratories) was used to avoid inhomogeneous broadening of the S-band EPR lines that would otherwise be present with the mixture of naturally occurring isotopes. S-band spectra (3.5 GHz) were acquired in D_2O solution at 133 K using a loop gap resonator as part of a specially designed spectrometer housed at the Biomedical ESR Center at the Medical College of Wisconsin. The $m_I = -1/2$ lines of these spectra were simulated using stick diagrams with Gaussian line shapes. Three pulse ESEEM measurements were obtained at 4.2 K on an X-band pulsed-EPR spectrometer. The instrument, cavity, and resonator were constructed in-house and have been previously described (24). Data were obtained at $g_\perp$, the point of greatest spectral intensity (3280 G at 9.47 GHz). Data processing to attain frequency domain spectra for 3-pulse ESEEM was carried out using software described in previous work (25). The HYSCORE pulse sequence was $\pi/2$-τ-$\pi/2$-t_1-π-t_2-$\pi/2$ (26). Data were processed using the software package WINEPR (Bruker). Experimental parameters for all pulsed experiments are provided in the figure legends.

Results

X-ray Crystallography

It has been demonstrated that the suboctarepeat segment HGGGW possesses all the functional groups that directly coordinate Cu^{2+} and thus constitutes the fundamental copper ion binding

site (4). The X-ray crystal structure (0.7 Å resolution) of HGGGW–Cu^{2+} was determined from crystals grown in pH 7.4 aqueous solution. Each unit cell contains a single HGGGW–Cu^{2+} complex along with six ordered water molecules. Figure 2a shows a stereo representation of the HGGGW–Cu^{2+} complex crystal structure with the electron density (blue) contoured at 2 σ. Additional density found by difference maps contoured at 3.5 σ reveals ordered hydrogens on the axially bound water (white). (Density arising from other ordered water molecules was omitted for clarity.) The detailed structure, shown in Figure 2b, reveals that the Cu^{2+} possesses a pentacoordinate environment with equatorial ligation from the δ1 nitrogen of the His imidazole and deprotonated amide nitrogens from the next two Gly residues. The second Gly also contributes its amide carbonyl oxygen. With the exception of the His backbone nitrogen and alpha carbon, all atoms from the His through to the nitrogen of the third Gly lie approximately in the equatorial plane and the copper is just above this plane, as consistent with a pentacoordinate complex.

The Trp indole also participates in the coordination environment, but in a rather unusual fashion. There is a water molecule axially bound to the copper. The indole nitrogen from the Trp side chain is 3.0 Å from the oxygen of this bound water, suggesting a hydrogen bond as indicated by a dashed line. This arrangement places the plane of the indole ring above the copper such that it is nearly parallel with the equatorial plane. Two additional water molecules hydrogen bond to the axial water forming a network extending from the backbone carbonyl preceding the His to the carbonyl of the third Gly.

The crystal structure also reveals hydrogen bond contacts between copper binding units as shown in Figure 2c for four HGGGW–Cu^{2+} units. The NH groups from the imidazole and Trp backbone position to form complementary hydrogen bonds to the backbone amide carbonyls of the His and the first Gly of the neighboring HGGGW segment, creating stable contacts between structured HGGGW–Cu^{2+} units.

Electron Paramagnetic Resonance

The constructs used for EPR studies are listed in Table 1. HGGGW is the fundamental Cu^{2+} binding unit, PHGGGWGQ is the consensus octarepeat, and PrP(23–28, 57–91) contains the full octarepeat domain (Figure 1). The string of basic residues KKRPKP, corresponding to PrP (23–28), is included in this latter construct to improve solubility. S-band EPR along with ^{15}N scanning was used to evaluate whether the equatorial coordination environment identified in Figure 2 is preserved in low-temperature aqueous solution for HGGGW and the PHGGGWGQ octarepeat. The benefit of S-band EPR arises from a partial cancellation of *g*-strain- and *A*-strain-induced inhomogeneous broadening specifically for the ^{63}Cu $m_I = -1/2$ hyperfine line (27). The $m_I = -1/2$ line of the low-frequency S-band (3.4 GHz) EPR spectrum reveals superhyperfine couplings from nitrogens directly coordinated to Cu^{2+} centers as seen in Figure 3 (27,28). We previously demonstrated that the couplings seen here in the top spectra are consistent with three ^{14}N couplings, in agreement with the equatorial coordination geometry of Figure 2 (4). Because ^{15}N possesses a different nuclear spin ($I = 1/2$) than ^{14}N ($I = 1$), site-specific ^{15}N labeling can be used to identify the directly coordinated nitrogens by an observed change in multiplet structure.

A series of HGGGW peptides was prepared with each member of the series ^{15}N-labeled at a unique glycine amide (Table 1). S-band EPR were obtained from samples in D_2O solution at measured pH = 7.4. Figure 3 shows the family of spectra down each column where the ^{15}N substitution is at the underlined glycine. The vertical lines drawn from the most prominent features of the spectra obtained from the unlabeled peptides are included to guide the eye and emphasize changes in multiplet patterns. For HGGGW, a change in multiplet structure relative to the unlabeled species is seen only for the first and second glycines, demonstrating that the nitrogens of these residues directly coordinate to the copper center, which is consistent with

the crystal structure. Interestingly, comparison of the spectra of HGGGW and HGGGW reveals slightly different coupling patterns, with the latter giving a wider separation among the most prominent lines. The origin of this difference is unclear but may reflect unequal Cu–N bond lengths from the first and second glycines to the copper center. Nevertheless, the qualitative change in multiplet patterns among the ^{15}N-labeled constructs demonstrates conclusively that only the first and second glycines directly coordinate to the copper center.

Simulations were employed using a previously described model (4) to determine whether the observed changes in multiplet structure with ^{15}N labeling are consistent with the hyperfine coupling constants determined previously. Although the ^{15}N scanning data here may suggest a slight inequivalence for the ligated nitrogen couplings, we previously showed that a simple model of three equivalent nitrogens (a_N = 13 G) and a single hydrogen (a_H = 10 G) is sufficient to reproduce the S-band EPR data (4) as shown in Figure 3. To incorporate the effect of ^{15}N labeling, one nitrogen spin was changed to I = 1/2 along with rescaling of the nuclear g value. The resulting simulation is shown in Figure 3 and indeed predicts the hyperfine structure observed for HGGGW and HGGGW.

All four glycines were individually labeled in a series of octarepeat peptides (Table 1), and the results are shown in Figure 3. Again, a change in multiplet structure is observed only for the first two glycines. The spectra shown in Figure 3 confirm that the nitrogen contacts to the copper identified for HGGGW are preserved in the octarepeat segment.

Finally, several attempts were made to obtain superhyperfine couplings from S-band spectra of PrP(23–28, 57–91). In all cases, no couplings were resolved. The $m_I = -1/2$ line was slightly broader than that obtained from the octarepeat and HGGGW, suggesting that inhomogeneous broadening was masking the desired multiplet pattern. Fully loaded PrP(23–28, 57–91) contains four Cu^{2+} ions (see Discussion), and, hence, weak dipolar interactions between the paramagnetic centers or structural inhomogeneities may contribute an additional source of inhomogeneous broadening that is not canceled in the $m_I = -1/2$ line at S-band.

ESEEM spectroscopy is a pulsed EPR technique that is sensitive to spin-active nuclei within approximately 10 Å of the paramagnetic copper center (29). For example, the method readily identifies imidazole coordination by detection of the remote nitrogen (30). In its application here, ESEEM serves as a complement to S-band EPR which detects directly coordinated nitrogens. ESEEM spectra were obtained for HGGGW and PHGGGWGQ, each with a single bound Cu^{2+}, and for PrP(23–28, 57–91) with four bound Cu^{2+} at pH = 7.4 and are shown in Figure 4a. These spectra reveal typical features that have been previously assigned to imidazole coordination (4,30), consistent with the crystal structure reported here. There is an additional set of peaks with prominent features, in particular, at 2.0 and 2.8 MHz. To assign these peaks, we used the library of ^{15}N-labeled peptides (Table 1). The ESEEM spectrum of HGGGW is shown in Figure 4b and reveals only those peaks assigned to the imidazole. [With the experimental conditions used here, 3-pulse ESEEM amplitudes of the quadrupolar ^{14}N nucleus are much greater than those of the dipolar ^{15}N nucleus (31) and thus peaks associated with this latter species are not observed in Figure 4.] All other ^{15}N-labeled HGGGW peptides gave spectra equivalent to that observed from the unlabeled species (data not shown). These observations demonstrate that the ^{14}N of the third glycine [Gly(3)] is responsible for the additional set of ESEEM peaks in HGGGW. To test this assignment in the full PrP octarepeat domain, a labeled analogue of PrP(23–28, 57–91) was prepared with ^{15}N-glycine at the Gly (3) position of all four octarepeats (specifically, PrP sequence positions 64, 72, 80, and 88; Table 1). ESEEM of PrP(23–28, 57–91, ^{15}N-64, 72, 80, 88) with four bound Cu^{2+} is shown in Figure 4b and is found to be equivalent to that obtained from HGGGW and reveals only those peaks assigned to the imidazole. In turn, this demonstrates that the nitrogen of Gly(3) is not

coordinated to the copper center either in HGGGW or in the corresponding positions in PrP (23–28, 57–91), in agreement with the crystal structure (Figure 2).

The low-frequency lines at 0.57, 0.90, and 1.47 MHz, which were previously assigned to the remote nitrogen of the imidazole (4), are characteristic of a weakly coupled ^{14}N nucleus close to the exact cancellation limit. This limit results from the cancellation of the vector sum of the ^{14}N nuclear Zeeman and hyperfine fields in one of the electron spin manifolds, and gives rise to ^{14}N quadrupolar transitions (denoted NQI for nuclear quadrupole interaction) (30). The ESEEM frequencies for these transitions are given by the following equations:

$$\begin{aligned} \nu_0 &= \frac{2\eta e^2 qQ}{4h} \\ \nu_+ &= \frac{e^2 qQ(3+\eta)}{4h} \\ \nu_- &= \frac{e^2 qQ(3-\eta)}{4h} \end{aligned} \quad (1)$$

where q is the z-component of the electric field gradient across the nucleus, Q is the ^{14}N quadrupole moment, η is the asymmetry parameter describing the x- and y-components of the electric field gradient across the nucleus, h is Planck's constant, and e is the electron charge.

In addition, ESEEM peaks are evident at ~0.8, 2.0, and 2.8 MHz. From ^{15}N scanning experiments, it is clear that these result from coupling to the noncoordinated amide nitrogen of Gly(3). Use of eq 1 to determine NQI parameters (e^2qQ/h and η) is valid only if these peaks can be considered predominantly quadrupolar in nature, e.g., the nucleus is at or near the condition of exact cancellation: $\nu_I = A_{iso}/2$, in which ν_I is the nuclear Larmor frequency and A_{iso} is the isotropic component of the hyperfine interaction (30). *A* property of quadrupole transitions near exact cancellation is that their frequency is largely insensitive to applied magnetic field strength (and corresponding EPR excitation frequency) (32,33). We investigated the field/EPR frequency dependence of these Gly(3) peaks by registering ESEEM patterns at 8.9 and 10.5 GHz (data not shown) in addition to the 9.47 GHz spectra shown in Figure 4. The low-frequency peaks assigned to Gly(3) exhibited little or no field dependence, indicating that their frequencies are primarily determined by the (field-independent) nuclear quadrupolar interaction. Use of eq 1 to determine e^2qQ/h and η yields values of 3.20 MHz and 0.50, respectively. Correlations observed in HYSCORE experiments (see below) provide further confirmation of this assignment and lead to an A_{iso} value of 1.41 MHz for this ^{14}N nucleus. Although this means that the condition of exact cancellation has not been precisely achieved at this magnetic field value (3280 G), it has been shown previously that ESEEM spectra of $I = 1$ nuclei display properties indicative of exact cancellation provided deviations from exact cancellation (defined by $\Delta = |2\nu_I - A_{iso}|$) are less than $e^2qQ/3h$ (32). For the spectra of the amide ^{14}N considered here, $\Delta = 0.61$ MHz $< e^2qQ/3h = 1.06$ MHz. This confirms the assignment of the spectra as at approximate exact cancellation and, together with the multifrequency and HYSCORE experiments, justifies the assignment of the ~0.8, 2.0, and 2.8 MHz peaks as quadrupolar and the use of eq 1 in determining e^2qQ/h and η.

The ESEEM spectrum of HGGGW (Figure 4b) reveals those transitions due solely to the remote nitrogen of the imidazole and thus allows for a more accurate determination of its quadrupolar parameters. The transitions and corresponding e^2qQ/h and η values are given in Table 2 and represent only a slight adjustment over that reported previously (4). The quadrupolar parameters are fully consistent with a remote nitrogen in the protonated state (30).

The quadrupolar parameters for the amide nitrogen of the third glycine in HGGGW were determined from the well-resolved ν_- and ν_+ peaks and are reported in Table 2. The values

e^2qQ/h = 3.2 MHz and η = 0.5 are very close to those observed for amide nitrogens of other O-coordinated glycine–metal ion complexes as determined by NQR spectroscopy (34). For example, the O-coordinated amide in the chloride and bromide salts of the Cd^{II}(Gly-Gly)-(imidazole) complex give quadrupolar parameters of e^2qQ/h = 3.22 MHz, η = 0.474 and e^2qQ/h = 3.20, η = 0.483, respectively. They are also in agreement with quadrupole parameters assigned to an amide nitrogen in azurin using ENDOR and ESEEM at 95 GHz (35) and HYSCORE at 9 GHz (36).

The two nitrogens giving rise to the ^{14}N ESEEM spectra are rigidly fixed in place by the coordination geometry shown in Figure 2. According to the crystal structure, the remote nitrogen of the imidazole and the amide nitrogen of the third glycine are 4.12 and 4.09 Å from the Cu^{2+}, respectively. The equivalence of the ESEEM spectra from HGGGW, the octarepeat, and PrP(23–28, 57–91) and their ^{15}N-labeled analogues indicates that the electronic and molecular structure of the environment of the two ^{14}N nuclei are similar for all three peptides. This finding, in turn, suggests that the equatorial coordination environment identified by the crystal structure is preserved in HGGGW, in the octarepeat, and in PrP(23–28, 57–91).

HYSCORE experiments allow for enhanced resolution of spectra complicated by the presence of multiple nuclei or significant anisotropic line broadening (26). The HYSCORE experiment represents an important orthogonal technique for confirming the relevance of the X-ray crystal structure to copper-bound HGGGW in solution. As was stated earlier, ESEEM suggests a common equatorial ligand sphere about the central copper. As an extension of the spin–echo experiment, HYSCORE provides a means to directly measure anisotropic hyperfine interactions and more definitively assign transitions to their parent nuclei (37).

In the HYSCORE sequence, the addition of a π pulse between the second and third $\pi/2$ pulses introduces correlations between nuclear spin coherences of opposing manifolds which, for the I = 1 exact cancellation case, links the NQI transitions of one electron spin manifold with the higher frequency double quantum transition in the opposite manifold (36). In addition, the appearance of an echo-modulation echo allows detection of anisotropically broadened ESEEM lines as observed for dipolar-coupled I = 1/2 species (26,37,38).

The HYSCORE spectra in Figure 5 were obtained with the same HGGGW samples studied in Figure 4. Figure 5a shows the spectra of the natural isotope HGGGW. Here, cross-peaks are observed between the NQI and DQ transitions for both the remote nitrogen of imidazole and the ^{14}N of Gly(3) previously assigned in 3-pulse ESEEM spectra. Those peaks assigned to the Gly(3) ^{14}N-amide in the ESEEM experiment are maintained in HYSCORE, and correlations between NQI and DQ lines in this experiment are consistent with the exact cancellation assignment (Figure 5a). Further, in the ^{15}N-substituted peptide HGG<u>G</u>W (Figure 5b), a new set of cross-peaks at 0.47 and 2.43 MHz are observed and replace those at 2.85 and 4.50 MHz. We assign these peaks, which are not resolved in 3-pulse ESEEM, to the I = 1/2 ^{15}N nucleus of Gly(3). The theoretical treatment of I = 1/2, S = 1/2 HYSCORE spectra appropriate for this case has been presented by Dikanov et al. (39). Assuming that the anisotropic component of the hyperfine interaction between an I = 1/2 nucleus and an S = 1/2 metal electron may be adequately described by the point dipole approximation, the hyperfine tensor for this system is axial with principal values of ($-T$, $-T$, 2T), and the shape of the cross-peaks is described by the equations:

$$\nu_\alpha{}^2 = Q\nu_\beta{}^2 + G \tag{2}$$

in which

$$Q=\frac{(T+2A_{\mathrm{iso}} \pm 4\nu_{\mathrm{I}})}{(T+2A_{\mathrm{iso}} \pm 4\nu_{\mathrm{I}})} \quad (3)$$

$$G=\pm 2\nu_{\mathrm{I}}\frac{(4\nu_{\mathrm{I}}{}^2 - A_{\mathrm{iso}}{}^2+2T^2 - A_{\mathrm{iso}}T)}{(T+2A_{\mathrm{iso}} \pm 4\nu_{\mathrm{I}})} \quad (4)$$

A_{iso} and T are, respectively, the isotropic and anisotropic components of the hyperfine coupling constant, ν_{I} is the nuclear Larmor frequency, ν_α and ν_β are nuclear frequencies of α and β spin manifolds, respectively, determined from the HYSCORE spectra, and Q and G are derived from the cross-peak contour line shapes. Analysis of the ν_α, ν_β cross-peaks of Figure 5b yields $Q = -0.205$ and $G = 1.39$. Solving eqs 2–4 with $\nu_{\mathrm{I}} = 1.42$ MHz yields $|T| = 0.18$ MHz and $A_{\mathrm{iso}}(^{15}\mathrm{N}) = 1.96$ MHz (corresponding to $A_{\mathrm{iso}} = 1.41$ MHz for ^{14}N). These values together with the quadrupole parameters obtained from the ^{14}N data (see above) are consistent with the assignment to a nonligated amide nitrogen as found in the crystal structure (40).

The spectral region near the proton Larmor frequency for the sample HGGGW–Cu^{2+} is displayed in Figure 5c. The peak observed arises from a proton(s) experiencing a predominantly dipolar interaction with $A_{\mathrm{iso}} \sim 0$ and $T \sim 2$ MHz. Peaks assigned to protons of equatorially coordinated water have been clearly observed in HYSCORE spectra of copper complexes (38, 41). These peaks are typically quite intense and span a 6–8 MHz range perpendicular to the diagonal. These HYSCORE studies, together with previous ENDOR studies (42), measure $T = 4.8$–5.2 MHz and $A_{\mathrm{iso}} \approx 0.7$–$2.2$ MHz for protons of equatorially coordinated water. We observe no peaks in Figure 5c or any other data which can be assigned to equatorially ligated water. This is consistent with the crystal structure of copper-bound HGGGW in which the equatorial ligands consist of three nitrogen atoms and one carbonyl oxygen. The protons of axially ligated water have been studied by ENDOR and assigned coupling values of $T = 3.7$ MHz and $A_{\mathrm{iso}} < 0.2$ MHz (42). The peak in Figure 5c is eliminated when the sample is prepared in D_2O, indicating it is solvent-exchangeable. It is possible that it may arise from an axially coordinated water, as observed in the crystal structure, but a definite assignment is difficult to make because other weakly coupled solvent-exchangeable protons may contribute to this peak. The main conclusion drawn from Figure 5c is that no equatorial water ligation is observed in the HGGGW–Cu^{2+} solution structure, in agreement with the crystal structure.

Discussion

We have obtained the crystal structure of the copper binding site within the HGGGW segment of the PrP octarepeat domain. The copper is coordinated by the His imidazole and deprotonated amides from the next two glycines within the HGGGW segment. The Trp indole also participates through a hydrogen bond to the axially coordinated water molecule. Low-frequency S-band EPR along with a library of ^{15}N-labeled peptides demonstrates that in HGGGW and PHGGGWGQ the first two glycines directly coordinate to the Cu^{2+}, consistent with the crystal structure. ESEEM and HYSCORE spectroscopy reveal the expected pattern for His imidazole coordination as well as an additional coupled ^{14}N which, using the ^{15}N-labeled peptides, is assigned to the noncoordinated amide nitrogen of the third glycine in HGGGW and the corresponding third glycine of each octarepeat in PrP(23–28, 57–91). These site-specific couplings revealed by the ensemble of EPR experiments on HGGGW, PHGGGWGQ, and PrP(23–28, 57–91) are fully consistent with the crystal structure of Figure 2. Within the copper binding segment HGGGW, our studies show that only Gly(3) does not directly interact with the Cu^{2+} or its axial water. Interestingly, examination of the octarepeat

sequences (e.g., Figure 1) shows that this is the only position that exhibits sequence variability (43).

In previous work, we found that Cu^{2+}-bound complexes of HGGGW and PrP(23–28, 57–91) X-band EPR spectra were almost indistinguishable from each other. In addition, titrations showed that HGGGW bound a single Cu^{2+} whereas PrP(23–28, 57–91), with four HGGGW repeats, bound approximately four Cu^{2+} ions. Analysis of the X-band EPR signal integrals further showed that there was no detectable magnetic coupling among the four Cu^{2+} in the fully bound PrP(23–28, 57–91). These findings lead to the proposal that each individual octarepeat binds a single Cu^{2+} within the HGGGW unit. Indeed, the crystal structure reported here demonstrates that HGGGW provides a five ligand coordination environment as often found for Cu^{2+} complexes. When considered along with the identical site-specific couplings for HGGGW, the octarepeat, and PrP(23–28, 57–91) as revealed by EPR here, these findings make a compelling argument for a structure where the fully copper-loaded octarepeat domain binds each Cu^{2+} in an HGGGW segment in a fashion equivalent to that of Figure 2.

Recent findings have led to speculation that PrP is a metal transporter. Pauli et al. found that copper stimulates the endocytosis of PrP (12). Deletion of the octarepeat domain eliminates this function (44). Brown has demonstrated that wild-type cells import more copper than do PrP knockouts (45). While we present no direct evidence to support the copper transport function for PrP, the steep pH-dependent binding of copper in the range of 6.0–7.4 (2,4), which represents the milieu of PrP in the endosome and on the cell surface, respectively, could indicate that the protein functions as a structural or biochemical switch, transducing information based on the level of bound copper and, in turn, on the concentration in the extracellular matrix. Interestingly the relatively weak affinity for copper (micromolar) may be akin to the constitutive glucose transporter whose K_d is on the order of the blood glucose concentration and is thus exceptionally sensitive in that range. That is, PrP may act as a cuprostat, activating cellular machinery in response to changes in ambient copper levels.

The specific PrP sequence HGGGW is highly conserved across species (43) and is found primarily within the prion family of proteins. The three-dimensional structure reported here represents a newly identified copper binding site. Previous structural work has demonstrated that the N-terminal domain of PrP^C, corresponding approximately to PrP(23–90), is unstructured in the absence of Cu^{2+} (46). The studies presented here suggest that in the physiological milieu, however, this region provides a novel Cu^{2+} binding domain that functions to bind the metal ion in a pH-dependent manner, so that the affinity is switched between the extracellular and endosomal pH range. The structure of the prion copper binding site provides a structural basis for the putative pH-dependent molecular switch that governs the uptake and release of Cu^{2+}. The glycine amide–Cu linkages are highly pH-sensitive and release the metal ion below pH 6.5–7.0 (47). Mass spectrometry studies reveal that indeed PrP(57–91), which contains four octarepeats, nevertheless binds only two copper ions with high affinity ($K_d < 5$ μM) at pH 6.0 (2). Pulsed EPR studies of PrP(23–231) at pH = 5.6 identify only imidazole coordination and no evidence of amide backbone coordination as observed here at extracellular pH 7.4 (6). The combined physiological and structural studies suggest a mechanism for PrP's function as a copper sensor or transporting protein that functions through endocytosis as shown schematically in Figure 6a (2,12). This mechanism is similar to that for iron transport by transferrin and the transferrin receptor (48). In the prion protein, however, the metal ion binding domain (the octarepeats) and the membrane-associated domain (the globular C-terminus with GPI anchor) are integrated into a single protein. Currently, there is no direct structural information as to how the octarepeat domain organizes at low endosomal pH or at low copper concentration. However, Viles et al. have suggested that at low [Cu^{2+}], copper ions are bound by two His imidazoles, thereby linking separate octarepeat segments (11).

Examination of the intermolecular contacts found in the crystal structure reveals a potentially important docking interaction between HGGGW–Cu^{2+} units that may explain PrP's cooperative copper binding. Figure 2c (see Results) shows four adjacent copper binding units as they are found in the crystal and illustrates how the fully copper-loaded octarepeat domain might be organized in the protein. To accommodate this type of octarepeat domain structure, the intervening -Gly-Gln-Pro- sequence must reach from the C-terminus of one HGGGW unit to the N-terminus of the next. Preliminary modeling studies suggest that this copper-induced stabilizing interaction can be achieved with sterically allowed backbone conformations. While we find that such a model is reasonable based on steric arguments, spectroscopic data suggest caution. The low-frequency components (<2.0 MHz) of imidazole ESEEM spectra are sensitive to the hydrogen bonding environment of the remote nitrogen (49). The similarity of these low-frequency features among the PrP segments suggests that the remote nitrogen experiences a hydrogen bonding environment that is equivalent in HGGGW, the octarepeat, and PrP(23–28, 57–91). Consequently, if PrP(23–28, 57–91) orders as suggested by Figure 2c, then buffer may act as the imidazole NH hydrogen bond acceptor for HGGGW and the octarepeat. Alternatively, HGGGW–Cu^{2+} units within PrP(23–28, 57–91) may organize in a yet unknown fashion that is distinct from that observed in the crystal.

It is noteworthy that within the octarepeat domain, glutamine is the only side chain possessing a functional group that does not participate in copper binding. Yet, this residue is highly conserved among mammalian PrPs (Figure 1). This observation may contribute to the understanding of PrP function. Recent work suggests that proteins with Gln/Asn-rich regions participate in regulatory processes through protein–protein contacts (50). Participation of octarepeat glutamine suggests an intermolecular recognition mechanism for PrP^{C} analogous to the glutamine zipper-mediated aggregation in Huntington's disease (51,52). When the octarepeat domain of PrP^{C} orders in the presence of copper, perhaps as suggested by the contacts within the crystal shown in Figure 2c, the glutamines are brought into close proximity to one another within the PrP N-terminal domain between HGGGW–Cu^{2+} units. These glutamine side chains may facilitate recognition between membrane-bound prion proteins through noncovalent interactions that stimulate endocytosis as shown in Figure 6b. Indeed, antibody cross-linked PrPs on cultured cells stimulate signal transduction (53), and it has been proposed that copper-induced oligomerization is a feasible mechanism for endocytotic trafficking of PrP (19). Glutamine cross-linked PrPs might occasionally allow interaction between the adjacent sequence PrP(90–120) on nearby PrPs as implicated in the formation of pathogenic PrP^{Sc} (54). Such a templating mechanism is consistent with that previously proposed in a study where additional octarepeats in some human family lines were found to confer predisposition to CJD (17). This concept may also help explain how copper converts PrP^{C} to a protease-resistant form (19).

The studies here have focused on copper binding in the octarepeat domain. However, recent work suggests that PrP possesses additional Cu^{2+} binding sites. Recombinant murine PrP with four octarepeats, nevertheless, binds five copper ions (23). Fluorescence and NMR experiments suggest an additional binding site involving histidines 96 and 111 in human PrP (55), and XAFS of PrP(91–231) supports the assignment of copper coordination by two histidines as well as a sulfur which is assigned to Met109 (56). In addition, aggregation of the neurotoxic peptide PrP(106–126) is highly metal ion dependent (57). How additional copper binding sites influence PrP function and copper binding in the octarepeat domain is yet to be determined.

Acknowledgments

We are grateful to Professors H. Ball, F. E. Cohen, and S. B. Prusiner (UCSF) for helpful discussion. In addition, the peptide PrP(23–28, 57–91), originally designed by H. Ball, was instrumental for obtaining high-quality EPR spectra of the octarepeat domain.

References

1. Prusiner SB. Proc Natl Acad Sci USA 1998;95:13363–13383. [PubMed: 9811807]
2. Whittal RM, Ball HL, Cohen FE, Burlingame AL, Prusiner SB, Baldwin MA. Protein Sci 2000;9:332–343. [PubMed: 10716185]
3. Brown DR, Qin K, Herms JW, Madlung A, Manson J, Strome R, Fraser PE, Kruck T, von Bohlen A, Schulz-Schaeffer W, Giese A, Westaway D, Kretzschmar H. Nature 1997;390:684–687. [PubMed: 9414160]
4. Aronoff-Spencer E, Burns CS, Avdievich NI, Gerfen GJ, Peisach J, Antholine WE, Ball HL, Cohen FE, Prusiner SB, Millhauser GL. Biochemistry 2000;39:13760–13771. [PubMed: 11076515]
5. Bonomo RP, Impellizzeri G, Pappalardo G, Rizzarelli E, Tabbi G. Chem–Eur J 2000;6:4195–4202.
6. Doorslaer SV, Cereghetti GM, Glockshuber R, Schweiger A. J Phys Chem B 2001;105:1631–1639.
7. Hornshaw MP, McDermott JR, Candy JM. Biochem Biophys Res Commun 1995;207:621–629. [PubMed: 7864852]
8. Miura T, Hori-i A, Mototani H, Takeuchi H. Biochemistry 1999;38:11560–11569. [PubMed: 10471308]
9. Prince RC, Gunson DE. Trends Biochem Sci 1998;23:197–198. [PubMed: 9644969]
10. Stockel J, Safar J, Wallace AC, Cohen FE, Prusiner SB. Biochemistry 1998;37:7185–7193. [PubMed: 9585530]
11. Viles JH, Cohen FE, Prusiner SB, Goodin DB, Wright PE, Dyson HJ. Proc Natl Acad Sci USA 1999;96:2042–2047. [PubMed: 10051591]
12. Pauly PC, Harris DA. J Biol Chem 1998;273:33107–33110. [PubMed: 9837873]
13. Klamt F, Dal-Pizzol F, da Frota MLC, Walz R, Andrades ME, da Silva EG, Brentani RR, Izquierdo I, Moreira JCF. Free Radical Biol Med 2001;30:1137–1144. [PubMed: 11369504]
14. Brown DR, Wong BS, Hafiz F, Clive C, Haswell SJ, Jones IM. Biochem J 1999;344(Pt 1):1–5. [PubMed: 10548526]
15. Brown DR. Trends Neurosci 2001;24:85–90. [PubMed: 11164938]
16. Bush AI. Curr Opin Chem Biol 2000;4:184–191. [PubMed: 10742195]
17. Goldfarb LG, Brown P, McCombie WR, Goldgaber D, Swergold GD, Wills PR, Cervenakova L, Baron H, Gibbs CJ Jr, Gajdusek DC. Proc Natl Acad Sci USA 1991;88:10926–10930. [PubMed: 1683708]
18. Flechsig E, Shmerling D, Hegyi I, Raeber AJ, Fischer M, Cozzio A, von Mering C, Aguzzi A, Weissmann C. Neuron 2000;27:399–408. [PubMed: 10985358]
19. Quaglio E, Chiesa R, Harris DA. J Biol Chem 2001;276:11432–11438. [PubMed: 11278539]
20. Vey M, Pilkuhn S, Wille H, Nixon R, DeArmond SJ, Smart EJ, Anderson RG, Taraboulos A, Prusiner SB. Proc Natl Acad Sci USA 1996;93:14945–14949. [PubMed: 8962161]
21. Waggoner DJ, Drisaldi B, Bartnikas TB, Casareno RL, Prohaska JR, Gitlin JD, Harris DA. J Biol Chem 2000;275:7455–7458. [PubMed: 10713045]
22. Peña MM, Lee J, Thiele DJ. J Nutr 1999;129:1251–1260. [PubMed: 10395584]
23. Kramer ML, Kratzin HD, Schmidt B, Romer A, Windl O, Liemann S, Hornemann S, Kretzschmar H. J Biol Chem 2001;276:16711–16719. [PubMed: 11278306]
24. Jiang F, McCracken J, Peisach J. J Am Chem Soc 1990;112:9035–9044.
25. Cornelius JB, McCracken J, Clarkson RB, Belford RL, Peisach J. J Phys Chem 1990;94:6977–6982.
26. Hofer P, Grupp A, Nebenfuhr H, Mehring M. Chem Phys Lett 1986;132:279–282.
27. Froncisz W, Hyde JS. J Chem Phys 1980;73:3123–3131.
28. Yuan H, Collins MLP, Antholine WE. J Am Chem Soc 1997;119:5073–5074.
29. Dikanov, SA.; Tsvetkov, YD. Electron spin–echo envelope modulation (ESEEM) spectroscopy. CRC Press; Boca Raton, FL: 1992.
30. Mims WB, Peisach J. J Chem Phys 1978;69:4921–4930.
31. Lai A, Flanagan HL, Singel DJ. J Chem Phys 1988;89:7161–7166.
32. Flanagan HL, Singel DJ. J Chem Phys 1987;87:5606–5616.
33. Flanagan HL, Gerfen GJ, Singel DJ. J Chem Phys 1988;88:20–24.

34. Ashby CIH, Paton WF, Brown TL. J Am Chem Soc 1980;102:2990–2998.
35. Coremans JWA, Vangastel M, Poluektov OG, Groenen EJJ, Denblaauwen T, Vanpouderoyen G, Canters GW, Nar H, Hammann C, Messerschmidt A. Chem Phys Lett 1995;235:202–210.
36. Kofman V, Farver O, Pecht I, Goldfarb D. J Am Chem Soc 1996;118:1201–1206.
37. Shane JJ, Hofer P, Reijerse EJ, De Boer E. J Magn Reson 1992;99:596–604.
38. Poppl A, Kevan L. J Phys Chem 1996;100:3387–3394.
39. Dikanov SA, Tyryshkin AM, Bowman MK. J Magn Reson 2000;144:228–242. [PubMed: 10828191]
40. Peloquin JM, Tang XS, Diner BA, Britt RD. Biochemistry 1999;38:2057–2067. [PubMed: 10026288]
41. van Gastel M, Bubacco L, Groenen EJJ, Vijgenboom E, Canters GW. FEBS Lett 2000;474:228–232. [PubMed: 10838090]
42. Atherton NM, Horsewill AJ. Mol Phys 1979;37:1349–1361.
43. Wopfner F, Weidenhöfer G, Schneider R, von Brunn A, Gilch S, Schwarz TF, Werner T, Schätzl HM. J Mol Biol 1999;289:1163–1178. [PubMed: 10373359]
44. Sumudhu W, Perera WS, Hooper NM. Curr Biol 2001;11:519–523. [PubMed: 11413003]
45. Brown DR. Biochem J 2000;352:511–518. [PubMed: 11085945]
46. Donne DG, Viles JH, Groth D, Mehlhorn I, James TL, Cohen FE, Prusiner SB, Wright PE, Dyson HJ. Proc Natl Acad Sci USA 1997;94:13452–13457. [PubMed: 9391046]
47. Sundberg RJ, Martin RB. Chem Rev 1974;74:471–517.
48. Aisen P, Wessling-Resnick M, Leibold EA. Curr Opin Chem Biol 1999;3:200–206. [PubMed: 10226041]
49. Colaneri MJ, Vitali J, Peisach J. Biochemistry 2000;39:584–591. [PubMed: 10642183]
50. Michelitsch MD, Weissman JS. Proc Natl Acad Sci USA 2000;97:11910–11915. [PubMed: 11050225]
51. Perutz MF, Johnson T, Suzuki M, Finch JT. Proc Natl Acad Sci USA 1994;91:5355–5358. [PubMed: 8202492]
52. Perutz MF. Trends Biochem Sci 1999;24:58–63. [PubMed: 10098399]
53. Mouillet-Richard S, Ermonval M, Chebassier C, Laplanche JL, Lehmann S, Launay JM, Kellermann O. Science 2000;289:1925–1928. [PubMed: 10988071]
54. Peretz D, Williamson R, Matsunaga Y, Serban H, Pinilla C, Bastidas R, Rozenshteyn R, James T, Houghten R, Cohen F, Prusiner S, Burton D. J Mol Biol 1997;273:614–622. [PubMed: 9356250]
55. Jackson GS, Murray I, Hosszu LL, Gibbs N, Waltho JP, Clarke AR, Collinge J. Proc Natl Acad Sci USA 2001;98:8531–8535. [PubMed: 11438695]
56. Hasnain SS, Murphy LM, Strange RW, Grossmann JG, Clarke AR, Jackson GS, Collinge J. J Mol Biol 2001;311:467–473. [PubMed: 11493001]
57. Jobling MF, Huang XD, Stewart LR, Barnham KJ, Curtain C, Volitakis I, Perugini M, White AR, Cherny RA, Masters CL, Barrow CJ, Collins SJ, Bush AI, Cappai R. Biochemistry 2001;40:8073–8084. [PubMed: 11434776]

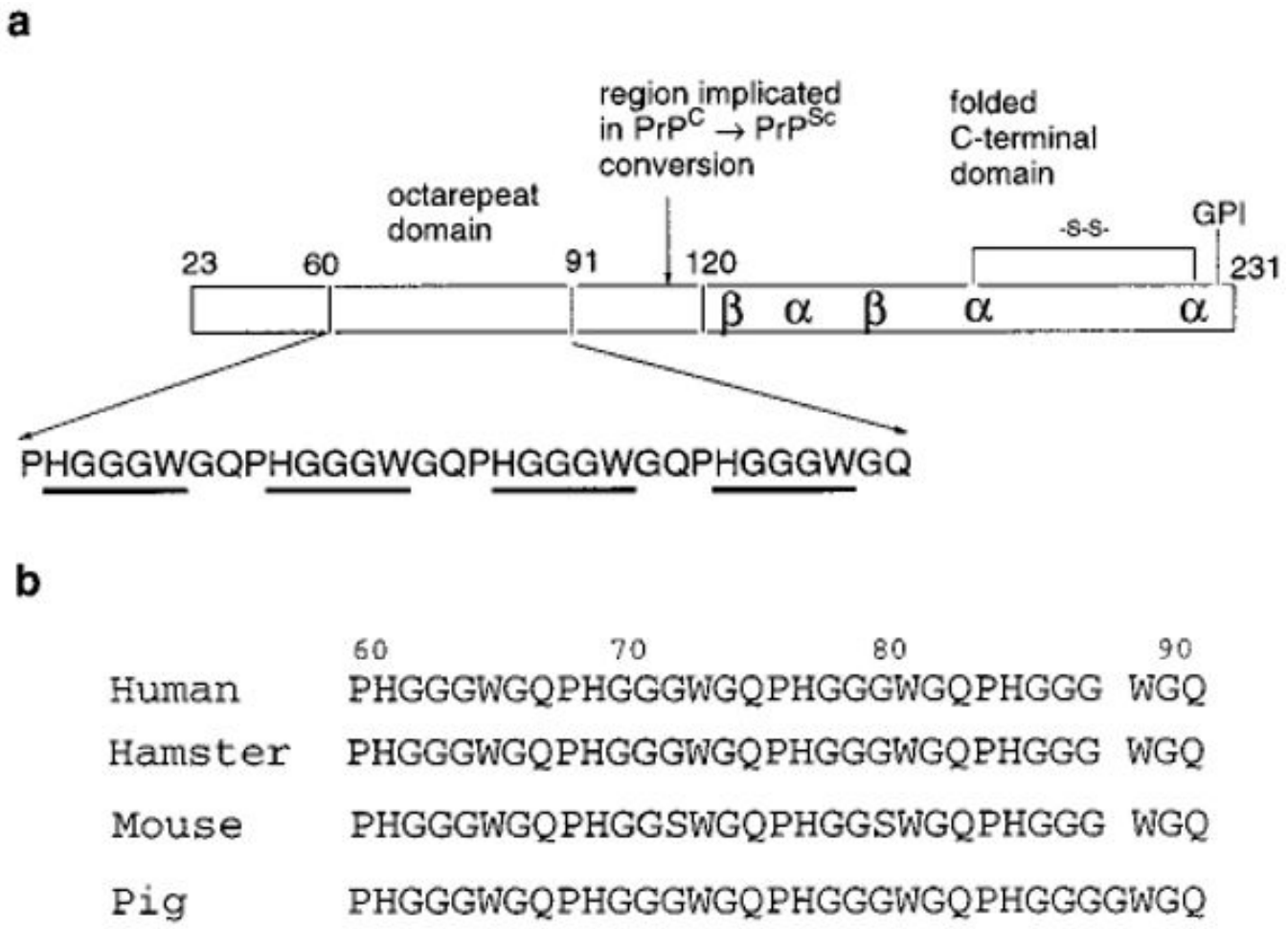

Figure 1.

Sequence of PrP and the octarepeat domain. (a) This sequence representation of PrP^C locates the globular C-terminal domain, the glycosylphosphatidylinositol (GPI) membrane anchor, and the octarepeat domain. Also shown is a flexible region implicated in multimerization that accompanies $PrP^C \rightarrow PrP^{Sc}$ conversion. Cu^{2+} binding within the octarepeats involves the specific residues HGGGW (underlined). (b) Alignment of the octarepeat domain from several species. Note that the only sequence variation within the HGGGW segments is either variation of the third glycine (to serine in two mouse octarepeats) or insertion of an additional glycine (in the porcine sequence).

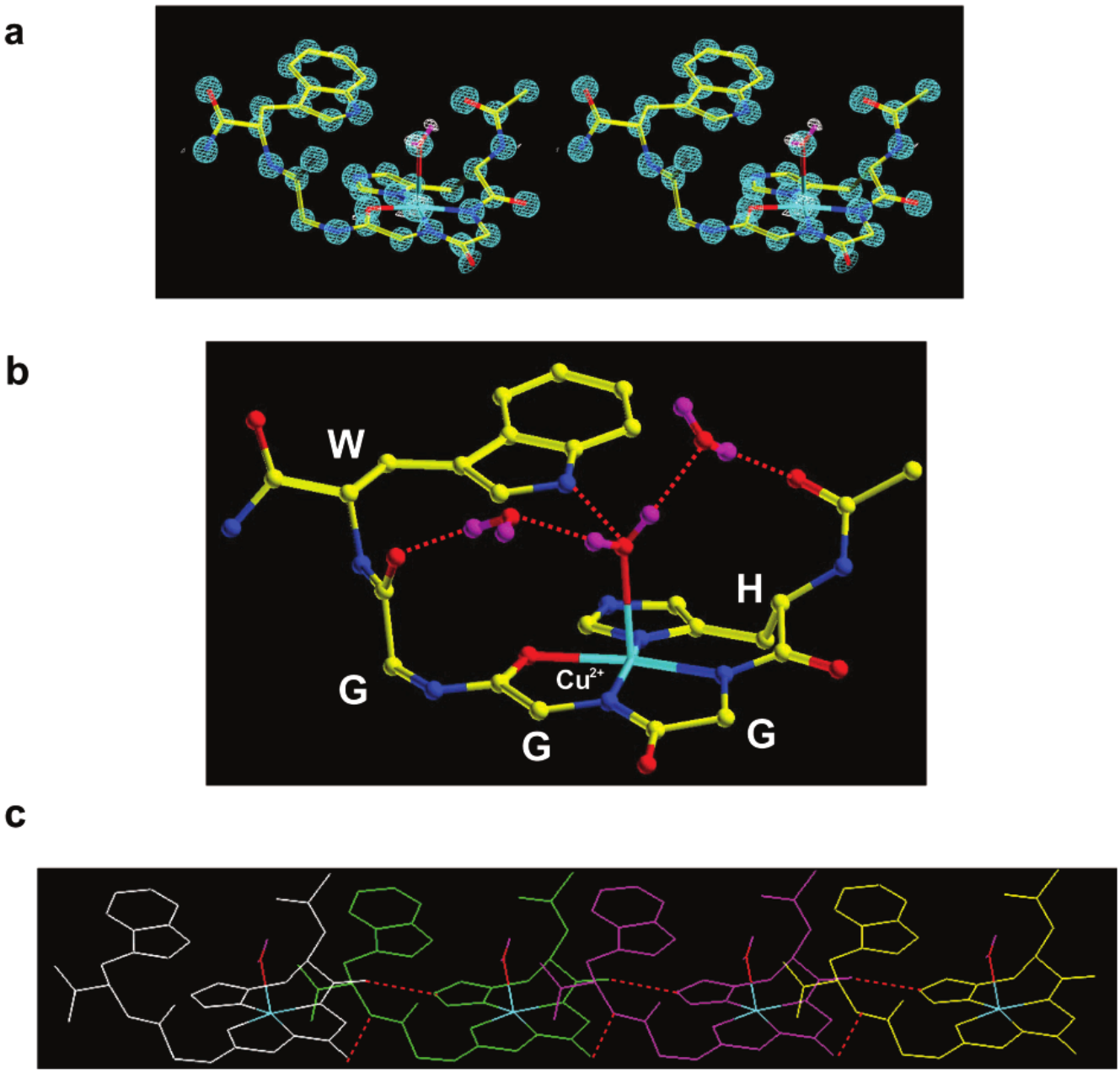

Figure 2.

Crystal structure (0.7 Å resolution) of the HGGGW segment in complex with Cu^{2+}. (a) A stereo representation of the electron density contoured at 2 σ is shown in blue. A difference map (white) reveals hydrogen density for the axially bound water. (b) This molecular representation shows how copper coordination is from the histidine imidazole and deprotonated amides from the next two glycines. In addition, the NH of the indole is within hydrogen bonding distance to the oxygen of the axial water. Two additional intramolecular ordered water molecules are also shown. (c) The red dashed lines show intermolecular hydrogen bond contacts identified in the crystal. These four copies of the copper binding units suggest a possible way in which the full octarepeat domain orders.

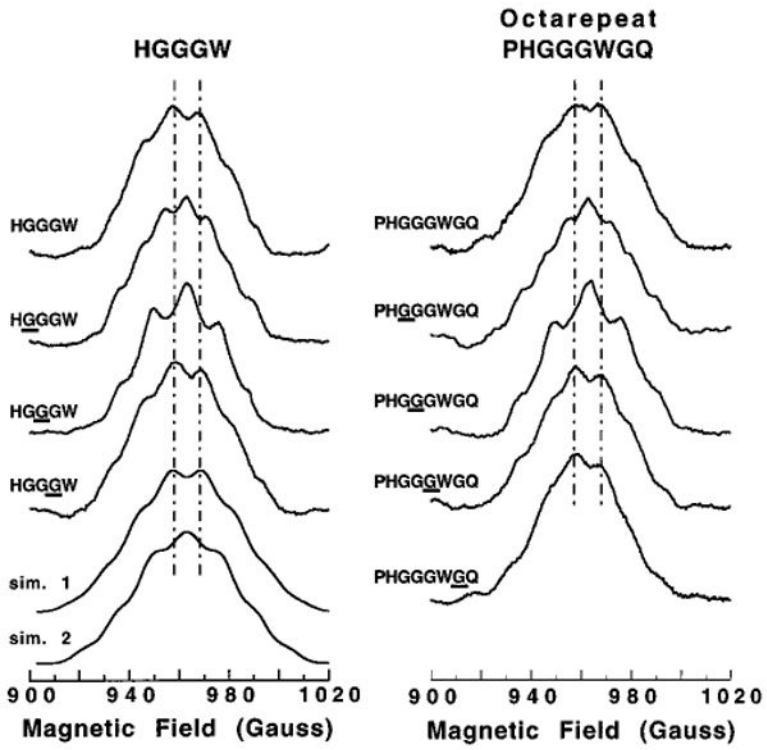

Figure 3.

The $m_I = -1/2$ line from the S-band EPR (3.5 GHz) of Cu^{2+} bound to ^{15}N-labeled HGGGW and PHGGGWGQ. For HGGGW, a change in multiplet structure is observed only when the first two glycines are ^{15}N-labeled, demonstrating that these nitrogens coordinate Cu^{2+}. The vertical lines drawn from the most prominent features of the unlabeled spectra are included to guide the eye. The bottom two spectra are simulations where sim. 1 is for three equivalent ^{14}N ($a_N = 13$ G) and a hydrogen ($a_H = 10$ G) and sim. 2 has one ^{14}N replaced with an ^{15}N. PHGGGWGQ shows the same pattern as HGGGW, indicating that the first two glycines coordinate to the copper center.

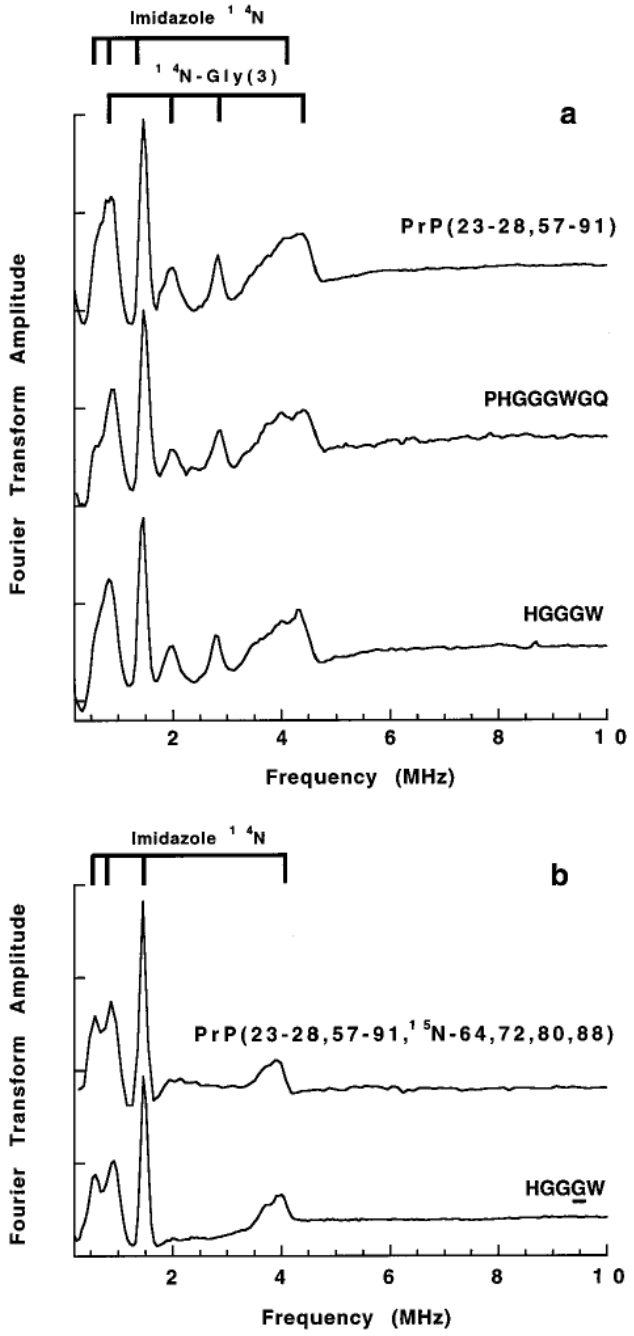

Figure 4.

Stimulated ESEEM spectra of HGGGW, PHGGGWGQ, and PrP(23–28, 57–91). (a) Spectra of unlabeled species with assignments, based on comparison to spectra obtained from the ^{15}N-labeled peptides (see panel b), shown by the grids at the top. All spectra from unlabeled constructs show coupling to the remote NH of the imidazole and a noncoordinated amide nitrogen. (b) These spectra of ^{15}N-labeled HGG<u>G</u>W and PrP(23–28, 57–91, ^{15}N-64,72,80,88) show only those transitions due to the remote NH of the His imidazole consistent with the finding that the third glycine in each HGGGW is not coordinated to the Cu^{2+}. Parameters for data acquisition were as follows: temperature, 4.2 K; $\pi/2$ pulse widths, 20 ns; repetition rate, 13 Hz; τ, 140 ns; T increment, 20 ns; 30 averages per point.

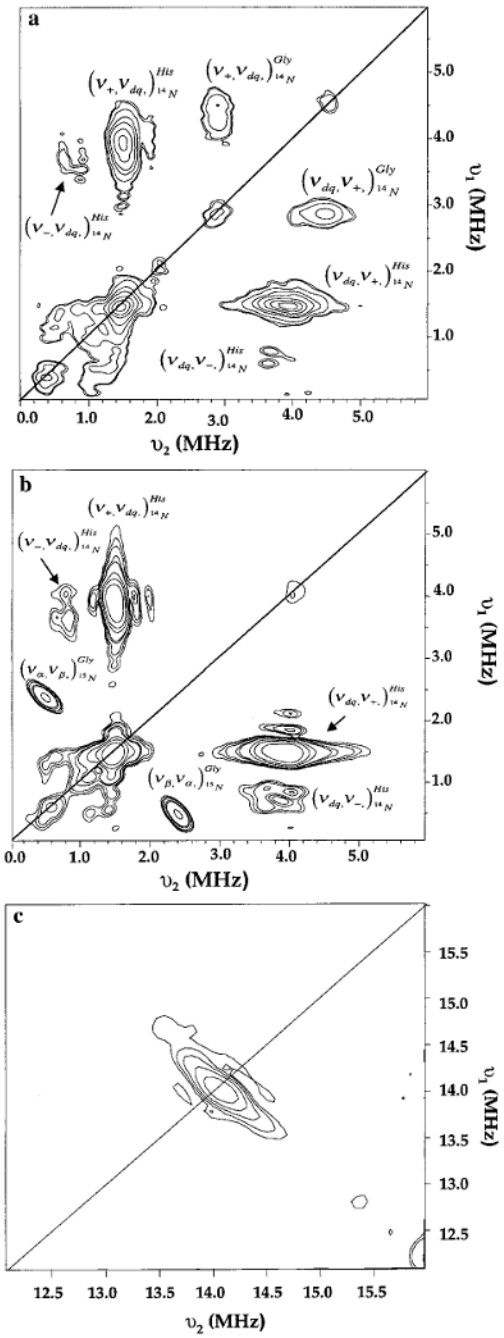

Figure 5.

HYSCORE spectra of HGGGW with (b) and without (a) ^{15}N-substitution at the third glycine amide. Peaks assigned to imidizole nuclear quadrupolar (NQI) and double quantum (DQ) transitions are correlated in the spectra and remain so after substitution of ^{15}N. In spectrum b, the glycine NQI and DQ features are lost and replaced by peaks at 0.47 and 2.43 MHz corresponding to a dipolar coupling to the metal center. Panel c shows the spectra consistent with weakly coupled protons. Parameters for data acquisition were as follows: temperature, 4.2 K; $\pi/2$ pulse widths, 20 ns; repetition rate, 53 Hz; τ, 160 ns; T increment, 40 ns; 40 averages per point. Initial $t_{1,2}$ = 40 ns, $t_{1,2}$ step = 40 ns.

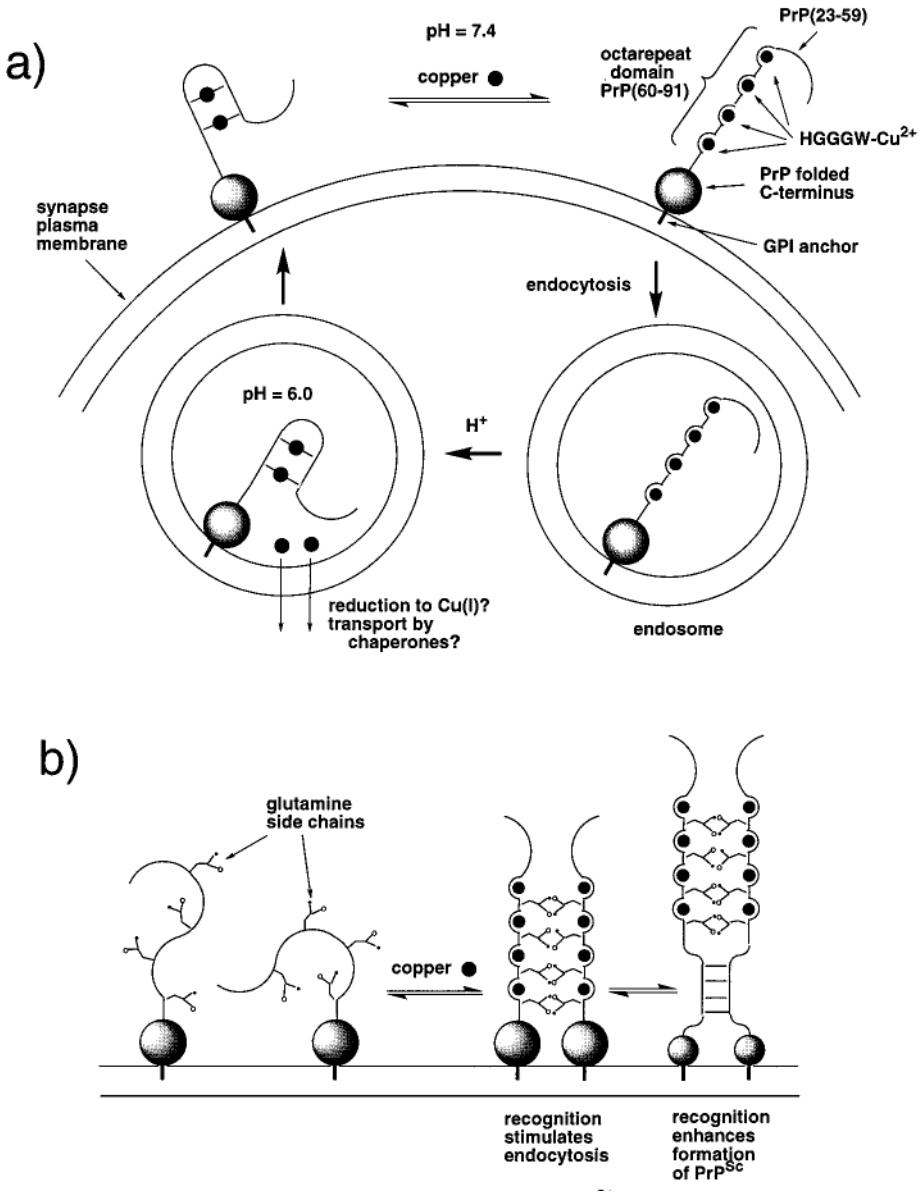

Figure 6.

Working hypotheses for how the prion protein functions to transport Cu^{2+} through endocytosis and how the octarepeat domain participates in the formation of pathogenic PrP^{Sc}. (a) At extracellular pH, each octarepeat binds a single Cu^{2+}. Within the endosome at pH ≈ 6.0, protonation of the amides competes with Cu^{2+} coordination, thereby lowering the affinity for the metal ion. There is no current information as to how PrP binds remaining Cu^{2+} at low pH; however, some experimental evidence points to multiple His coordination (see Discussion). (b) The glutamines in each octarepeat do not participate in Cu^{2+} coordination yet are highly conserved in mammalian prions. Copper orders the octarepeat domain at pH 7.4 bringing the glutamines into close proximity to one another. The Gln side chains facilitate intermolecular recognition between neighboring, membrane-bound PrPs. This noncovalent cross-linking may be a molecular signal that stimulates endocytosis or transmembrane signaling. When accompanied by rare events leading to partial unfolding of the globular domain, the cross-

linked species allows for recognition between PrPs in the adjacent region PrP(90–120), thereby facilitating formation of PrP^{Sc}.

Table 1

PrP-Derived Peptide Sequences

HGGGW	Ac-His-Gly-Gly-Gly-Trp-NH_2
H<u>G</u>GGW	Ac-His-Gly(^{15}N)-Gly-Gly-Trp-NH_2
HG<u>G</u>GW	Ac-His-Gly-Gly(^{15}N)-Gly-Trp-NH_2
HGG<u>G</u>W	Ac-His-Gly-Gly-Gly(^{15}N)-Trp-NH_2
PHGGGWGQ	Ac-Pro-His-Gly-Gly-Gly-Trp-Gly-Gln-NH_2
PH<u>G</u>GGWGQ	Ac-Pro-His-Gly(^{15}N)-Gly-Gly-Trp-Gly-Gln-NH_2
PHG<u>G</u>GWGQ	Ac-Pro-His-Gly-Gly(^{15}N)-Gly-Trp-Gly-Gln-NH_2
PHGG<u>G</u>WGQ	Ac-Pro-His-Gly-Gly-Gly(^{15}N)-Trp-Gly-Gln-NH_2
PHGGGW<u>G</u>Q	Ac-Pro-His-Gly-Gly-Gly-Trp-Gly(^{15}N)-Gln-NH_2
PrP(23–28, 57–91)[a]	Ac-KKRPKPWGQPHGGGWGQPHGGGWGQPHGGGWGQPHGGGWGQ-NH_2
PrP(23–28, 57–91, ^{15}N-64,72,80,88)[a,b]	Ac-KKRPKPWGQPHGG<u>G</u>WGQPHGG<u>G</u>WGQHGG<u>G</u>WGQPHGG<u>G</u>WGQ-NH_2

[a] The sequences of these peptides are represented using the single-letter amino acid code.

[b] This peptide incorporates ^{15}N-labeled glycines at positions 64, 72, 80, and 88.

Table 2

^{14}N ESEEM Transitions[a]

	ν_0	ν_-	ν_+	e^2Qq/h	h
imidazole remote NH	0.570	0.900	1.47	1.58	0.72
Gly(3) amide NH	(0.8)	2.00	2.80	3.20	0.50

[a] All frequencies are reported in MHz.